Wideband design of compact monopole-Like circular patch antenna using modal analysis

Nie, Liying; Lau, Buon Kiong; Xiang, Shang; Aliakbari Abar, Hanieh; Wang, Bao; Lin, Xian Qi

Published in:
IEEE Antennas and Wireless Propagation Letters

DOI:
10.1109/LAWP.2021.3066985

2021

Document Version:
Peer reviewed version (aka post-print)

Wideband Design of Compact Monopole-Like Circular Patch Antenna Using Modal Analysis

Li Ying Nie, Buon Kiong Lau, *Senior Member, IEEE*, Shang Xiang, Hanieh Aliakbari, Bao Wang, Xian Qi Lin, *Senior Member, IEEE*

***Abstract*—In this paper, we present a systematic approach to design a compact dual-mode monopole-like patch antenna using characteristic mode analysis (CMA). The modal analysis of a slotted circular patch structure incorporating a new shorting pin loading technique is presented. To achieve a compact monopole-like antenna with wideband operation, it is demonstrated that the first two significant modes with monopole-like patterns are the most suitable ones for dual-mode excitation. Based on the analysis of the modal currents and electric fields, four groups of shorting pins and four slots are introduced to individually tune the two modes, which facilitates the optimization. The effects of these slots and shorting pins on the resonant frequencies of the two modes are analyzed in detail. Finally, a CPW T-junction power divider is applied to simultaneously excite these two modes and suppress the undesired modes. Apart from a more compact form factor and higher gain than existing work, it also features a competitive gain-bandwidth per volume ratio.**

***Index Terms*—Compact antenna, multimode antenna, patch antenna, characteristic mode analysis**

I. Introduction

ANTENNAS with monopole-like radiation patterns are widely used in wireless communication systems, such as indoor wireless networks and vehicle communication networks [1], [2]. To reduce the size of wireless devices, compact and low-profile monopole-like microstrip patch antennas with low cost and easy fabrication were developed in the past two decades to replace the conventional monopole antenna [3]-[12].

Most of the patch antennas in the literature are analyzed and designed with cavity model theory [4]-[10]. For circular patch antenna, TM_{01} and TM_{02} modes are commonly used to produce monopole-like radiation patterns. Monopole-like circular antennas based on $TM_{01,}$ TM_{02} or TM_{22} mode are excited by coaxial cables or an L-probe feed in [4]-[7]. To simultaneously excite the TM_{01} and TM_{02} modes to achieve a larger bandwidth, a set of concentrically-distributed conductive pins is introduced in the circular patch antennas in [8] and [9]. A tri-mode monopole-like patch antenna is designed in [10] by exciting the TM_{01} and TM_{02} modes of the patch and the TM_{02} mode of the parasitic ring. Multi-element antenna analyzed by the diakoptic theory is also used to achieve the dual-resonant monopole antenna (so-called Goubau antenna) in [11]-[12]. However, its profile is relatively high compared with printed patch antennas.

Although the cavity model theory can be utilized to approximate the resonant frequencies of the cavity modes of a regular patch antenna structure, it is more challenging to find the conventional cavity modes for irregular patch structures, e.g., those with added slots and shorting pins. Recently, characteristic mode analysis (CMA) is becoming more and more attractive for antenna analysis and synthesis due to the feed-independent insights it offers on regular/irregular structures' resonance properties [13]-[25]. Therefore, CMA has become a versatile tool in the analysis and design of different antenna types, especially antennas with irregular structure. In this context, CMA can also be applied to provide the modes of the modified structure with shorting pins and slots.

This paper explores the design of a compact dual-mode circular patch antenna with improved shorting pin and slot loading techniques under the guidance of CMA. Based on the analysis of the modal current and electric field distributions of the patch with one shorting pin, two monopole-like modes with the lowest resonant frequencies are chosen to realize a more compact antenna than other mode combinations used in the existing literature. Individually mode control is realized by introducing four groups of shorting pins and four slots. In addition, a CPW T-junction is used to simultaneously excite the two modes with monopole-like pattern and suppress the modes with broadside pattern. Good agreement between the measured and simulated results verifies the feasibility of using the new combination of modes to design the compact dual-mode monopole-like antenna under the guidance of CMA.

II. Antenna Design and Analysis

A. Mode Analysis and Selection

It was shown in [9] that the TM_{01} mode is the lowest order mode in the center-shorted circular patch that can produce a monopole-like pattern. Therefore, a circular patch loaded with one shorting pin in the center (see Fig. 1 (a)) is first analyzed with theory of characteristic mode (TCM). The radius of the pin

Manuscript received August 30, 2020. (*Corresponding author: Liying Nie*)

Li Ying Nie is with the School of Computer Science and Information Engineering, Hefei University of Technology, Hefei 230601, China (*E-mail: liyingnie@sina.com).

Buon Kiong Lau, Hanieh Aliakbari, Shang Xiang are with the Department of Electrical and Information Technology, Lund University, Lund 22100, Sweden.

Xian Qi Lin, Bao Wang are with the EHF Key Lab of Fundamental Science, School of Electronic Engineering, , Chengdu 611731, China (E-mail: xqlin@uestc.edu.cn).

is 0.5 mm. The substrate used in the simulation is lossless F4B with the thickness of 2 mm and the relative permittivity of 2.5. The initial radius of the circular patch is set to be 23 mm, calculated by the approximate equation in [9] and [26], assuming that the center frequency is 3.5 GHz and the second lowest monopole-like mode resonates at 3.8 GHz. Except when indicated, the analysis in this part is carried out by using the multilayer solver of CST Studio Suite 2018.

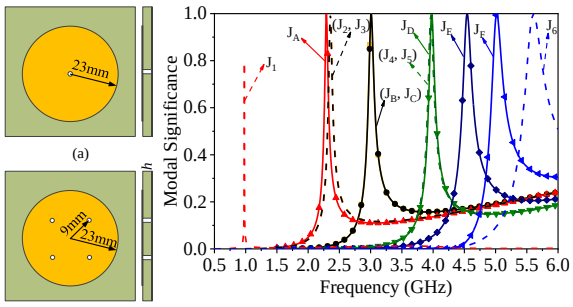

Fig 1. Circular patches with shorting pins and corresponding modal significance. (a) patch with one pin, (b) patch with four pins, (c) modal significance of the CMs (dashed line: patch with one pin, solid line with symbol: patch with four pins).

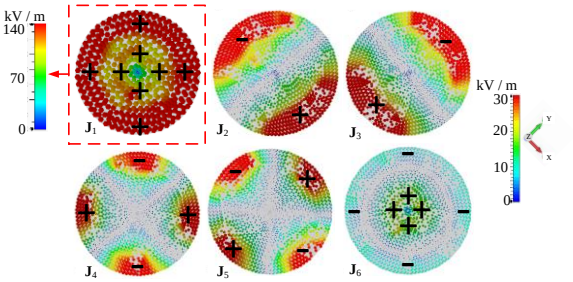

Fig. 2. Electric field distributions (1 mm below the patch) at the resonant frequencies of the first six modes of the circular patch with one shorting pin. "+" and "–" indicate the directions of the electric field.

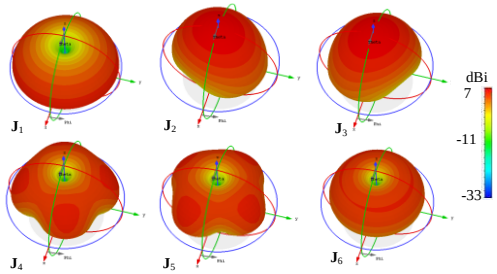

Fig. 3. Directivity at the resonant frequencies of the first six modes of the circular patch with one shorting pin.

The modal significances of the first six CMs of the patch with one shorting pin (Fig. 1(a)) are shown in Fig. 1(c), as indicated by $\mathbf{J}_1$ to $\mathbf{J}_6$. The corresponding electric fields (1 mm below the patch) and far-field patterns of these modes are given in Figs. 2 and 3, respectively. It can be seen that, except for the $\mathbf{J}_2$ and $\mathbf{J}_3$ modes, the radiation patterns of the other four modes are all monopole-like. Since the resonant frequencies of $\mathbf{J}_1$ and $\mathbf{J}_4$ ($\mathbf{J}_5$) modes are lower than $\mathbf{J}_6$ mode, if $\mathbf{J}_1$ and $\mathbf{J}_4$ ($\mathbf{J}_5$) modes are used in a dual resonance design, the overall dimensions of the antenna will be the smallest among different pairs of these four modes. Because $\mathbf{J}_4$ and $\mathbf{J}_5$ are modes which have same eigenvalues but orthogonally polarized within the entire frequency band according to TCM, only $\mathbf{J}_4$ is chosen to be excited together with $\mathbf{J}_1$ using a single excitation in this paper.

To draw the resonances of the $\mathbf{J}_1$ and $\mathbf{J}_4$ modes closer to each other, more shorting pins should be introduced to increase the resonant frequency of $\mathbf{J}_1$ [8], [9]. Based on the electric field distribution of $\mathbf{J}_4$ in Fig. 2, four shorting pins were placed symmetrically around the center in the area with the weak electric field of $\mathbf{J}_4$ (shown in Fig. 1 (b)) to avoid disturbing the $\mathbf{J}_4$ mode. The central pin is removed here because it has little effect on the two selected modes after the four pins are added. The placement of the shorting pins is different from the design in [9] that uses 19 pins. The corresponding modes (i.e., $\mathbf{J}_1$ to $\mathbf{J}_6$) after introducing the four pins are denoted as $\mathbf{J}_A$ to $\mathbf{J}_F$ (see Fig. 1(c)). Except for the $\mathbf{J}_4$ and $\mathbf{J}_6$ modes, the resonant frequencies of all the other modes are shifted upwards after using the four shorting pins. For $\mathbf{J}_4$, the shorting pins located at its null-voltage regions would not affect its resonant frequency. On the other hand, the resonant frequency of $\mathbf{J}_6$ is shifted downwards due to the perturbation introduced by the shorting pins [9].

B. Excitation Method

To selectively excite a monopole-like radiation pattern, the feed is designed to excite the $\mathbf{J}_A$ and $\mathbf{J}_D$ modes while suppressing the broadside $\mathbf{J}_B$ and $\mathbf{J}_C$ modes (whose resonant frequencies are between the $\mathbf{J}_A$ and $\mathbf{J}_D$ modes). Figure 4 shows the electric field distributions of $\mathbf{J}_A$ to $\mathbf{J}_D$ just under the patch with four shorting pins. To selectively excite the $\mathbf{J}_A$ and $\mathbf{J}_D$ modes and suppress the $\mathbf{J}_B$ and $\mathbf{J}_C$ modes, two equal-amplitude and in-phase feeds should be applied around the points **B** and **B'** in Fig. 4.

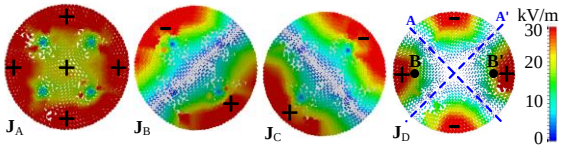

Fig. 4. Electric field distributions (1 mm below the patch) at the resonant frequencies of the $\mathbf{J}_A$ to $\mathbf{J}_D$ modes of the circular patch with four shorting pins. "+" and "–" indicate the directions of the electric field.

To obtain good impedance matching (i.e., reflection coefficient ≤ -10 dB) for the proposed antenna together with the feeding structure, the locations of the two in-phase feeding points were optimized along the line connecting **B** and **B'**.

C. Mode Adjustment Using Shorting Pins and Slots

From the analysis above, to achieve a larger impedance bandwidth with dual resonances, more shorting pins should be used to tune $\mathbf{J}_A$ towards $\mathbf{J}_D$. Further analysis concerning the effect of shorting pins on the two modes was performed using CMA, as described below.

Because the electric field strength along the **A** and **A′** line sections of the $\mathbf{J}_D$ mode is weak (as shown in Fig. 4), introducing shorting pins along these two lines do not have much effect on $\mathbf{J}_D$. However, $\mathbf{J}_A$ will be greatly affected due to its significant electric field strength along these lines, as depicted in Fig. 4. Figure 5 shows the effect of the shorting pins on the $\mathbf{J}_A$ and $\mathbf{J}_D$ modes. When d =17.3 mm and g is kept the

same, the resonant frequency of $\mathbf{J}_A$ increases with the increase in the number of the shorting pins (N) in each group (see Fig. 5(a)). The maximum resonant frequency of the $\mathbf{J}_A$ mode is around 3 GHz. However, the resonant frequency of the $\mathbf{J}_D$ mode is almost unchanged, since the positions of the shorting pins correspond to the null-voltage points of the $\mathbf{J}_D$ mode but not the $\mathbf{J}_A$ mode. Similar phenomenon is observed when g changes. When the shorting pins ($N \geq 3$) are moved towards the edge, the resonant frequency of the $\mathbf{J}_A$ mode increases (see Fig. 5(b)). With the increase of N, the frequency shift becomes more obvious.

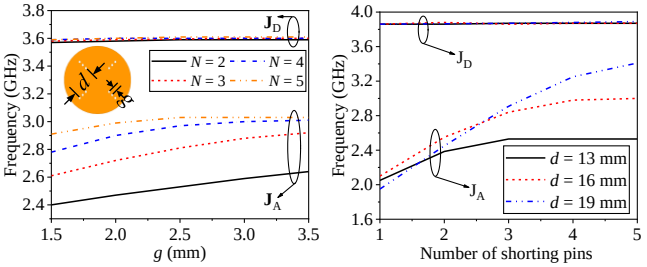

(a) (b)

Fig. 5. Effects of the shorting pins on the resonant frequencies of $\mathbf{J}_A$ and $\mathbf{J}_D$ modes. (a) d = 17.3 mm, (b) g = 3 mm

Apart from shorting pins, slots can also be applied to decrease the resonant frequency of $\mathbf{J}_D$, to move the resonances of $\mathbf{J}_A$ and $\mathbf{J}_D$ closer to each other. As shown in Fig. 6(a), all the modal currents on the patch of $\mathbf{J}_A$ flow from the edge towards the shorting pins and most of them are along the radial directions. However, for $\mathbf{J}_D$, most of the currents are along the phi direction. Therefore, loading slots along radial direction at the current's maximum point on the edge will increase the current path length of the $\mathbf{J}_D$ mode and consequently lower its resonant frequency, but it will have little effect on the $\mathbf{J}_A$ mode.

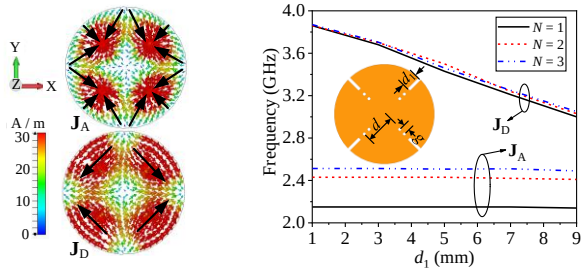

(a) (b)

Fig. 6. (a) Modal current at the resonant frequencies of the $\mathbf{J}_A$ and $\mathbf{J}_D$ modes of the circular patch with four shorting pins and (b) the effect of slots on the resonant frequencies of the $\mathbf{J}_A$ and $\mathbf{J}_D$ modes with different numbers of radially aligned shorting pins N (g = 3 mm, d = 13 mm).

The cases of the patch antenna with different numbers of radially aligned shorting pins (N = 1, 2 and 3) around each of the original four shorting pin positions are studied (see Fig. 6(b)). The resonant frequency of $\mathbf{J}_D$ decreases from 3.87 GHz to 3.03 GHz due to the increased current path length, when d_1 varies from 1 to 9 mm and N = 2. However, the resonant frequency of $\mathbf{J}_A$ only increases very slightly. The same phenomenon is observed when the number of the shorting pin changes.

The above analysis reveals that $\mathbf{J}_A$ and $\mathbf{J}_D$ can be individually tuned and parameters relating to the shorting pins and the slots are further optimized to lower the frequency of $\mathbf{J}_D$ and increase

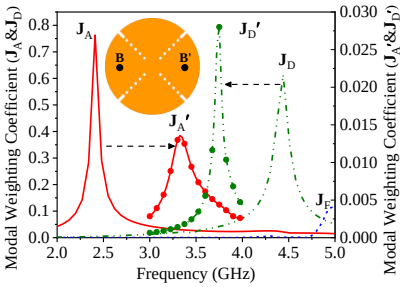

Fig. 7. Magnitude of modal weighting coefficients for the circular patch fed by two equal-amplitude and in-phase feeding ports at **B** and **B'** before and after mode adjustment. (g = 3 mm, d = 17.5 mm, and d_1 = 3.8 mm. The modal weighting coefficients of the $\mathbf{J}_B$ and $\mathbf{J}_C$ modes are almost zero and not shown.)

that of $\mathbf{J}_A$. Figure 7 shows the comparison of the magnitude of the modal weighting coefficients directly extracted from simulation results with the multilayer solver of Altair FEKO 2018 for the circular patches before and after adjustment, fed by two equal-amplitude and in-phase wire feeding ports located at the points **B** and **B'**, with the distance of 36 mm. The radius of the shorting pins is 0.7 mm. As can be seen, for the patch with four shorting pins (Fig. 1(b)), the $\mathbf{J}_A$ and $\mathbf{J}_D$ modes dominate the radiation at the lower and higher frequencies, respectively, while the $\mathbf{J}_B$ and $\mathbf{J}_C$ modes hardly radiate with these two in-phase feeding ports. Compared with those of the patch in Fig. 1(b), the resonant frequencies of the $\mathbf{J}_A$ and $\mathbf{J}_D$ modes have shifted from 2.41 and 4.43 GHz to 3.38 GHz ($\mathbf{J}_A'$) and 3.7 GHz ($\mathbf{J}_D'$), respectively, after introducing 20 pins and four slots.

III. Proposed Antenna and Experimental Results

A. The Proposed Antenna

According to the above analysis, the optimal geometry of the proposed antenna is shown in Fig. 8. The antenna is confined within $0.54\lambda \times 0.54\lambda \times 0.023\lambda$ at the center frequency of 3.5 GHz, where λ is the free-space wavelength. A single layer F4B substrate with the relative permittivity of 2.55, loss tangent of0.002 and thickness of 2 mm is used in the design. The circular patch etched with four symmetrical slots is printed on the top of the substrate. Four groups of shorting pins with each group radial-arrayed are used to connect the patch to the ground.

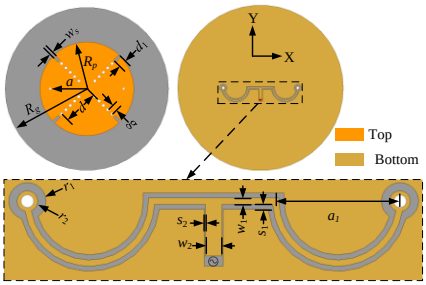

Fig. 8. Geometry of the proposed circular patch antenna. (R_g = 50 mm, R_p = 23 mm, a = 18 mm, d = 17.5 mm, d_1 = 3.8 mm, w_s = 1.5 mm, g = 3 mm, r_1 = 1.8 mm, r_2 = 1 mm, a_1 = 12 mm, s_1 = 0.5 mm, s_2 = 0.1 mm, w_1 = 0.6 mm, w_2 = 1.6 mm).

The radius of all the pins is 0.7 mm. A CPW T-junction power divider is printed in the ground layer to feed the circular patch. The two output ports of the T-junction power divider are

connected to the patch by two metal vias with the radius of 0.6 mm. The dimensions of the T-junction are optimized with the conventional Finite Element Method (FEM) solver in 2018 Ansys HFSS to improve the impedance matching of the patch.

B. Experimental Results and Discussion

To verify the design, a prototype is fabricated, as shown in Fig. 9. The substrate used in the fabrication is the same as that of the simulation in Section III-A. Figure 10(a) shows the reflection coefficient of the fabricated antenna. The measured result reveals that the operating bandwidth is from 3.21 to 3.64 GHz ($|S_{11}|$< 10 dB), which is slightly wider than the simulated bandwidth due to fabrication tolerances.

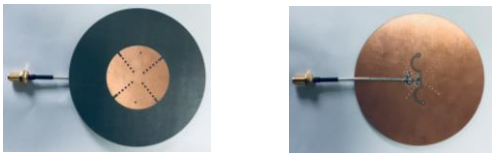

(a) (b)

Fig. 9. Photograph of the fabricated antenna. (a) front view, (b) back view.

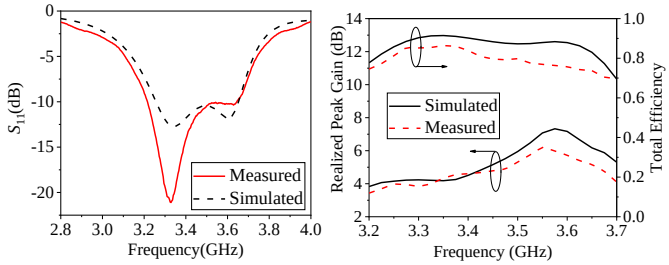

(a) (b)

Fig 10. Simulated and measured S-parameters, realized peak gain and efficiency of the proposed antenna.

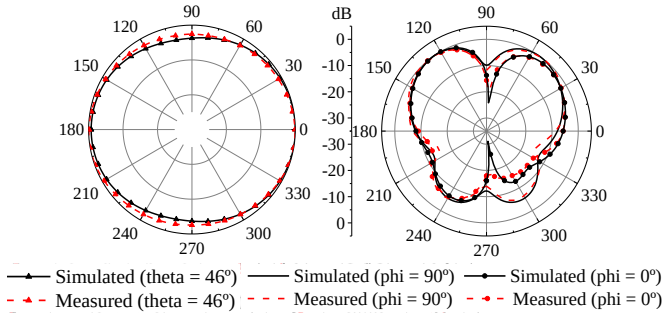

Fig 11. Simulated and measured normalized radiation patterns at 3.5 GHz.

The radiation patterns of the fabricated antenna are measured with a SATIMO near-field measurement system. In the operating bandwidth, the maximum measured realized peak gain and total efficiency are 6.23 dB and 86% (-0.66 dB), respectively (see Fig. 10(b)). Good agreements are obtained between the simulation and measured gain and efficiency values. The simulated and measured normalized radiation patterns at 3.5 GHz are given in Fig. 11, showing good agreement with each other. It shows that the antenna produces an omnidirectional radiation pattern with 2.7 dB variation at theta = 46°, chosen as a reference elevation angle around the realized peak gain, which is also more attractive for base station antenna on the ceiling for indoor wireless communication. The gain variation of the pattern (for theta = 46°) is due to the application of the $\mathbf{J}_D$ mode and the adopted feeding network. The feeding network also results in the pattern asymmetry for phi = 0°, as confirmed in simulation. The mutual influence can be avoided by replacing CPW T-junction by a microstrip line divider isolated from the patch by the ground plane.

Comparisons between the proposed antenna and other monopole-like patch antennas are given in Table I. It can be seen that all the dual-mode antennas in the papers in Table I are designed using one or both of the TM_{01} and TM_{02} modes. However, the dimensions of these patch antennas are relatively large in order to support the TM_{02} mode. Based on the insights yielded by CMA, the $\mathbf{J}_A$ (TM_{01}) and $\mathbf{J}_D$ (TM_{21}) modes of the proposed patch design are employed in this work to obtain a more compact antenna size with a larger G×BW/(100V) of 22.1. Another advantage of the proposed design is the independent control of the two modes by using the new loading method of the shorting pins and slots (see Figs. 5 and 6).

To further explore the comparison with the circular patch antenna in [9], additional simulations are performed. It is found that if the effective radius (R_{eff}) of the circular patch antenna in [9] is reduced to that of the proposed antenna by increasing the permittivity of the substrate from 2.33 to 3.7, its bandwidth will decrease to that of the proposed antenna. This result highlights that the proposed antenna is not only more compact for a *given* substrate material, it also offers similar bandwidth even if another design is given the advantage of using a different substrate material (of higher permittivity). It is further noted that even though other types of antennas with monopole-like pattern can offer larger bandwidths (e.g., the travelling-wave antenna in [27]), patch antennas are suitable for applications requiring low-profile, low-cost and simple structure.

TABLE I
COMPARISON OF THE PROPOSED AND OTHER MONOPOLE-LIKE ANTENNAS

Ref.	Operating modes	Independent control	H (λ_g)	R_{eff} (λ_g)	G (dB)	BW (%)	G×BW (%) /100V (λ_g)
[6]	TM_{02}	/	0.05	1.056	5.7	12.8	2.7
[8]	TM_{01} TM_{02}	No	0.045	0.6	5.7	20	14.6
[9]	TM_{01} TM_{02}	No	0.037	0.575	5.5	18	16.6
[10]	TM_{01} TM_{02}	No	0.029	1.062	5.7	27.4	9.9
This work	**$\mathbf{J}_A$ ($\mathbf{TM_{01}}$) $\mathbf{J}_D$ ($\mathbf{TM_{21}}$)**	**Yes**	**0.037**	**0.441**	**6**	**12.55**	**22.1**

H: total height of antenna; λ_g: guide wavelength of the center frequency; R_{eff}: effective radius of the patch in [26]; G: measured realized peak gain at center frequency; BW: bandwidth; V: volume

IV. CONCLUSION

A monopole-like patch antenna is designed with a new combination of two cavity modes based on CMA. The modal properties reveal that four groups of radial-arrayed shorting pins and four slots can be used to effectively tune the resonant frequencies of two monopole-like modes. Independent mode control can be realized due to the application of the TM_{21} mode, which simplifies the final design optimization. Based on the analysis of the modal currents and electric fields, a CPW T-junction is used to excite/suppress the available modes. The proposed dual-resonance compact monopole-like antenna with high gain is suitable for indoor wireless communications.

REFERENCES

[1] W. Lin, H. Wong, and R. W. Ziolkowski., "Wideband pattern-reconfigurable antenna with switchable broadside and conical beams," *IEEE Antennas Wireless Propag. Lett.*, vol. 16, pp. 2638-2641, 2017.

[2] N. Nguyen-Trong, A. Piotrowski, T. Kaufmann, and C. Fumeaux, "Low-profile wideband monopolar UHF antennas for integration onto vehicles and helmets," *IEEE Trans. Antennas Propag.*, vol. 64, no. 6, pp. 2562-2568, 2016.

[3] S. Liu, W. Wu, and D. G. Fang, "Wideband monopole-like radiation pattern circular patch antenna with high gain and low cross-polarization," *IEEE Trans. Antennas Propag.*, vol. 64, no. 5, pp. 2042-2045, 2016.

[4] L. Economou, and R. J. Langley, "Patch antenna equivalent to simple monopole," *Electron. Lett.*, vol. 33, no. 9, pp. 727-729, 1997.

[5] Y. X. Guo, M. Y. W. Chia, Z. N. Chen and K. M. Luk, "Wide-band L-probe fed circular patch antenna for conical-pattern radiation," *IEEE Trans. Antennas Propag.*, vol. 52, no. 4, pp. 1115-1116, Apr. 2004.

[6] A. Al-Zoubi, F. Yang, and A. Kishk, "A broadband center-fed circular patch-ring antenna with a monopole like radiation pattern," *IEEE Trans. Antennas Propag.*, vol. *57, no.* 3, pp. 789-792, 2009.

[7] P. Mei, S. Zhang, X. Q. Lin and G. F. Pedersen, "A Low-Profile Patch Antenna With Monopole-Like Radiation Patterns," in *Proc. IEEE Antennas Propag. Soc. Int. Symp.*, Granada, Spain, 2019, pp. 1-3.

[8] Q. Hou, H. Tang, Y. Liu, and X. Zhao, "Dual-frequency and broadband circular patch antennas with a monopole-type pattern based on epsilon-negative transmission line," *IEEE Antennas Wireless Propag. Lett.*, vol. 11, pp. 442-445, 2012.

[9] J. Liu, Q. Xue, H. Wong, H. W. Lai, and Y. Long, "Design and analysis of a low-profile and broadband microstrip monopolar patch antenna," *IEEE Trans. Antennas Propag.*, vol. 61, no. 1, pp. 11-18, 2013.

[10] J. Liu, S. Zheng, Y. Li, and Y. Long, "Broadband monopolar microstrip patch antenna with shorting vias and coupled ring," *IEEE Antennas Wireless Propag. Lett.*, vol. 13, pp. 39-42, 2014.

[11] G. Goubau, N. Puri, and F. Schwering, "Diakoptic theory for multielement antennas," *IEEE Trans. Antennas Propag*., vol. 30, no. 1, pp. 15-26, Jan. 1982.

[12] C. B. Ravipati and S. R. Best, "The Goubau multi element monopole antenna-revisited," in *Proc. IEEE Antennas Propag. Soc. Int. Symp.*, Honolulu, HI, Jun. 9-15, 2007 pp. 233-236.

[13] Z. Miers, H. Li, and B. K. Lau, "Design of bandwidth-enhanced and multiband MIMO antennas using characteristic modes," *IEEE Antennas Wireless Propag. Lett.*, vol. 12, pp. 1696-1699, 2013.

[14] H. Li, Z. T. Miers, and B. K. Lau, "Design of orthogonal MIMO handset antennas based on characteristic mode manipulation at frequency bands below 1 GHz," *IEEE Trans. Antennas Propag.*, vol. 62, no. 5, pp. 2756-2766, 2014.

[15] C. Deng, Z. Feng, and S. V. Hum, "MIMO mobile handset antenna merging characteristic modes for increased bandwidth," *IEEE Trans. Antennas Propag.*, vol. 64, no. 7, pp. 2660-2667, 2016.

[16] E. Antonino-Daviu, M. Cabedo-Fabrés, M. Sonkki, N. M. Mohamed-Hicho, and M. Ferrando-Bataller, "Design guidelines for the excitation of characteristic modes in slotted planar structures," *IEEE Trans. Antennas Propag.*, vol. 64, no. 12, pp. 5020-5029, 2016.

[17] F. H. Lin and Z. N. Chen, "Low-profile wideband metasurface antennas using characteristic mode analysis," *IEEE Trans. Antennas Propag.*, vol. 65, no. 4, pp. 1706-1713, 2017.

[18] F. H. Lin and Z. N. Chen, "Truncated impedance sheet model for low-profile broadband nonresonant-cell metasurface antennas using characteristic mode analysis," *IEEE Trans. Antennas Propag.*, vol. 66, no. 10, pp. 5043-5051, Oct. 2018.

[19] Z. Liang, J. Ouyang, F. Yang, and L. Zhou, "Design of license plate RFID tag antenna using characteristic mode pattern synthesis," *IEEE Trans. Antennas Propag.*, vol. 65, no. 10, pp. 4964-4970, 2017.

[20] B. Yang and J. J. Adams, "Computing and visualizing the input parameters of arbitrary planar antennas via eigenfunctions," *IEEE Trans. Antennas Propag.*, vol. 64, no. 7, pp. 2707-2718, Jul. 2016.

[21] Y. Wen, D. Yang, H. Zeng, M. Zou and J. Pan, "Bandwidth enhancement of low-profile microstrip antenna for MIMO applications," *IEEE Trans. Antennas Propag.*, vol. 66, no. 3, pp. 1064-1075, March 2018.

[22] M. Khan and D. Chatterjee, "Characteristic mode analysis of a class of empirical design techniques for probe-fed, U-slot microstrip patch antennas," *IEEE Trans. Antennas Propag.*, vol. 64, no. 7, pp. 2758-2770, Jul. 2016.

[23] Y. K. Chen and C. F. Wang, "Characteristic-mode-based improvement of circularly polarized U-slot and E-shaped patch antennas," *IEEE Antennas Wireless Propag. Lett.* vol. 11, pp. 1474-1477, 2012.

[24] C. Zhao and C. Wang, "Characteristic mode design of wide band circularly polarized patch antenna consisting of H-shaped unit cells," *IEEE Access*, vol. 6, pp. 25292-25299, 2018.

[25] H. Alroughani, "Studying microstrip patch antennas using the theory of characteristic modes," in *Proc. IEEE Antennas Propag. Soc. Int. Symp.*, Vancouver, Canada, Jul. 19-24, 2015, pp. 1476–1477.

[26] C. Shen, S. A. Long, M. R. Allerding, and M. D. Walton, "Resonant frequency of a circular disk, printed circuit antenna," *IEEE Trans. Antennas Propag.*, vol. AP-25, no. 4, pp. 595–596, Jul. 1977.

[27] A. A. Omar and Z. Shen, "A compact and wide-band vertically polarized monopole antenna," IEEE Trans. Antenna Propag., vol. 67, no. 1, pp. 626-631, Jan. 2019.